In-plane seismic behaviour of retrofitted masonry walls subjected to subsidence-induced damage

Drougkas, Anastasios; Licciardello, Lucia; Rots, Jan G.; Esposito, Rita

DOI
10.1016/j.engstruct.2020.111192

Publication date
2020

Document Version
Final published version

Published in
Engineering Structures

Engineering Structures 223 (2020) 111192

Contents lists available at ScienceDirect

Engineering Structures

journal homepage: www.elsevier.com/locate/engstruct

In-plane seismic behaviour of retrofitted masonry walls subjected to subsidence-induced damage

Anastasios Drougkas*, Lucia Licciardello, Jan G. Rots, Rita Esposito

Faculty of Civil Engineering and Geosciences, TU Delft, Stevinweg 1, 2628 CN Delft, the Netherlands

ARTICLE INFO

Keywords:
Unreinforced masonry
Induced seismicity
Subsidence-induced damage
Repair and strengthening
Digital image correlation

ABSTRACT

The province of Groningen in the Netherlands is experiencing the continuous impact of gas extraction in the form of induced seismicity. Due to the absence of naturally occurring seismicity in the region, the historic building stock of Groningen was constructed without empirical design features typically encountered in naturally seismic regions. Further, gas extraction, in combination with soft topsoil, is responsible for substantial amounts of ground subsidence. This subsidence may compromise the capacity of existing structures to bear seismic loading.

Historic masonry structures, particularly those lacking traditional earthquake-resistant features, are vulnerable to seismic loads. Further, their substantial weight, in-plane stiffness, low tensile strength and brittleness renders them vulnerable to settlement-induced damage. Given the cultural significance of architectural heritage, the performance of historic buildings in the Damage Limitation (DL) state is a matter of importance. Additionally, due to the incorporation of both vernacular and monumental architectural heritage buildings in the urban setting, their performance in the Near Collapse (NC) state is as important as that of ordinary building structures. Therefore, methods and techniques for enhancing the behaviour of historic buildings in both States need to be devised and evaluated.

This paper focuses on the application and assessment of a retrofitting technique commonly used for damage prevention and repair in unreinforced masonry structures in the Netherlands, namely bed joint reinforced repointing. The technique consists in the embedment of stainless-steel bars in continuous bed joints, as well as their dry placement across cracks in the masonry. The technique is applied on a masonry wall tested under quasi-static cyclic in-plane shear loading for the evaluation of its performance not only in the DL state for which it was conceived, but also in the NC states. The wall features artificially introduced cracks that simulate settlement-induced damage prior to the installation of the bars.

A finite element meso-model is used for the simulation of the wall tests, featuring the artificial damage and reinforcement elements. The model is used in non-linear cyclic analyses for the simulation of the experiments.

Through experimental testing and numerical modelling, the efficiency of the strengthening technique is evaluated in terms of resulting shifts in wall capacity, stiffness and failure mode. Further comments are provided concerning its applicability and structural compatibility.

1. Introduction

1.1. State of the art

The link between gas extraction and induced seismicity has been clearly established over the last decades [1]. Earthquake activity from gas extraction, while of relatively low magnitude, occurs at high frequency. Repetitive seismic loading may gradually compromise the load-bearing capacity of building structures through the accumulation of light damage and reduction of durability.

In addition to earthquake induction, soil subsidence may arise due to gas extraction, particularly in areas of soft soil [2]. Buildings on subsiding or uplifting soil may suffer aesthetic or structural damage due to soil-structure interaction caused by the different elastic stiffness of the soil and the superstructure-foundation system [3].

Both seismic action and soil-structure interaction result in in-plane loading of masonry panels. Seismic action, depending primarily on the location of the excitation source and the orientation of the masonry panel, additionally results in out-of-plane action. The response of masonry panels to in-plane action, including the expected failure mode, is dependent on numerous parameters, such as boundary conditions, vertical load, compressive/tensile/shear strength and structural

* Corresponding author.
E-mail address: A.Drougkas@tudelft.nl (A. Drougkas).

https://doi.org/10.1016/j.engstruct.2020.111192
Received 11 May 2020; Received in revised form 14 July 2020; Accepted 28 July 2020

typology [4]. Unreinforced masonry (URM) structures, due to their high weight, high structural stiffness, low tensile strength and low ductility are especially vulnerable to both subsidence-induced damage and earthquake action [5,6].

Both the in-plane seismic behaviour and response to soil settlement of masonry structures has been extensively studied. Experimental and numerical work on the seismic response of solid clay brick masonry, primarily consisting in cyclic testing of masonry piers, is relatively abundant in the literature. More complex tests, featuring panels with openings and accompanied by the determination of the material properties of masonry, are less frequent [7–9]. Similarly, a substantial body of work is encountered on the subject of subsidence-induced damage [10–12]. However, the combined effect of subsidence and earthquake action has not been extensively studied.

Existing and historic masonry structures require special attention in the investigation of their resilience against light damage as well as of their safety against moderate or high seismic loads. Aesthetic damage due to, for example, soil subsidence, needs to be limited for reasons of preservation of the heritage value of the object and for reasons of maintaining durability, which is often compromised in historic buildings due to lack of maintenance. Further, in the case of induced seismicity, particularly in regions with no history of major naturally-occurring seismicity, historic masonry buildings will typically not include earthquake-resistant features encountered in seismically active regions.

The Dutch province of Groningen is characterized by the coincidence of several features: a) extensive gas extraction operations, b) soft sop-soil, c) historic lack of seismic activity and d) a preponderance of historic masonry structures. The combination of these features has resulted in wide-spread damage to existing structures in the region, the vast majority of which appears to be linked to in-plane effects [13].

The performance of unreinforced masonry structures under earthquake action may be enhanced through retrofitting with bar-type reinforcement. Although promising, bed joint reinforced repointing has received limited attention in research literature, particularly as regards application in full-scale shear walls. These bars may be plain steel, stainless steel or Fibre-Reinforced Polymer (FRP) strips. The bars are usually placed in horizontal grooves in continuous bed joints, which are subsequently repointed, or vertically in grooves passing through both units and mortar joints. In order to reduce disturbance of the masonry during cutting and to reduce labour, these bars are typically mounted near the surface of the masonry member, in a one- or two-sided configuration. Results on small masonry panels tested in shear induced by diagonal compression [14,15] or in panels under combined vertical and shear force [16] generally report a small to moderate increase of the peak force, a reduction in diagonal cracking and an increase in ductility. In these cases, out-of-plane deformation has been reported for one-sided application in panels loaded in-plane.

To counteract the effects of subsidence-induced damage in Groningen, a strengthening technique consisting in the embedment of stainless-steel reinforcement bars in repointed bed joints, also known as bed joint reinforced repointing, has seen extensive use. A high strength mortar is used for the repointing, providing high strength and stiffness and an excellent bond with the reinforcement bars. This intervention technique, while having seen widespread use over several decades, has not been the subject of rigorous experimental and numerical investigation, especially at the structural scale. The potential of this technique for enhancing the in-plane performance of retrofitted masonry walls, thus dealing with both major structural issues faced in Groningen at once, is a further motivating factor for its investigation and improvement.

1.2. Objectives and methodology

In this paper the vulnerability of masonry structures to in-plane earthquake action is investigated. A widely-applied intervention method for the repair of subsidence-induced damage, namely bed joint reinforced repointing, is evaluated. Due to the peculiarities of induced seismicity, emphasis is placed on the Damage Limitation state. Damage limitation refers to the state where a structure has sustained visible, light but repairable damage.

The investigation was executed through experimental testing [17,18] and numerical simulation [19] at different levels of detail. A masonry wall with an opening, representative of the typologies found in Groningen [20], was tested first under a sequence of low amplitude repetitive cycles to induce “light damage” and subsequently tested up to the Near Collapse state. Near collapse refers to the state where a structure has sustained heavy damage tantamount to life-threatening collapse. A second wall was tested under similar conditions but was strengthened prior to being tested up to Near Collapse. Typical pre-existing subsidence-induced damage was included for the strengthened wall by creating non-bonded joints during the construction of the wall. Companion tests were carried out for the characterization of the properties of the materials. The intervention technique was numerically modelled using meso-scale non-linear finite element analyses. Shifts in the stiffness, capacity and failure mode due to the intervention were investigated.

2. Experimental campaign

The main objective of the experimental campaign is the assessment of bed joint reinforced repointing used in brick masonry walls. This strengthening method consists in the embedment of helical stainless-steel bars in continuous bed joints of masonry walls, which are repointed with a high strength mortar. The bars are vertically spaced at a distance depending on their location placed in wall. The repointed joints may extend in areas previously damaged by soil-subsidence or earthquake action or may extend in areas without damage. Additional helical anchors were placed diagonally in drilled holes across diagonal cracks, running through both units and mortar joints.

The constituent materials used in this campaign were: a) the units, b) the construction mortar, c) the repair mortar and d) the helical bars. All the materials were delivered in single batches and were mechanically characterized. Additional mechanical tests were executed for the determination of the tensile and shear bond of the unit-construction mortar interface as well as of the compressive and flexural strength of the masonry composite.

The in-plane behaviour of masonry is evaluated through in-plane shear-compression testing of full-scale walls. The walls include a single window opening and were tested under cyclic displacement.

2.1. Companion material tests

This subsection reports the companion material tests used to determine the properties of both construction and strengthening materials. For more information, the reader is referred to [21].

2.1.1. Units

The units for the construction of the masonry wall were solid clay bricks with dimensions $210 \times 50 \times 100\text{mm}^3$ (length $\times$ height $\times$ thickness). The compressive strength of the units was determined according to the relevant EN standard [22]. The tests were carried out in displacement control and the peak stress was appropriately scaled according to the shape factor of the bricks. The flexural strength of the units was determined according to the relevant Dutch standard [23]. The standard proposes a three-point bending test, with the unit loaded on the stretcher face. These tests were carried out in displacement control. Finally, the Young’s modulus of the units was measured through compression of stacked prisms with thin layer joints made of high-strength mortar [24]. Displacement measurements were registered using multiple Linear Variable Differential Transformers (LVDTs) spanning across 3 and 5 joints, as well as with short-span LVDTs placed in a single unit, all arranged in the direction of the load.

2.1.2. Construction mortar

Through the term "construction mortar" is meant the regular mortar used for the construction of the joints in the masonry specimens. For the sake of brevity, this material will be generally referred to in subsequent instances simply as "mortar". The mortar consisted of Ordinary Portland cement, hydrated lime and fine sand. The final mix proportions in weight were 1: 2: 9 (cement:lime:sand), corresponding to the typical proportions of an O-type cement-lime mortar [25]. This mortar is generally suitable for historic masonry due to mechanical compatibility and has an expected compressive strength of roughly 2.4N/mm^2 at 28 days.

Standard $160 \times 40 \times 40$mm^3 prismatic mortar specimens were produced for mechanical testing, with a minimum of 3 specimens produced each day of construction of masonry specimens. These specimens were stored in controlled conditions and tested after a minimum of 28 days. Three-point bending and compression tests were performed according to the relevant EN standard [26].

2.1.3. Masonry composite

Masonry specimens were constructed in running bond using the provided bricks and mortar for the determination of the mechanical properties of the masonry composite. Compression tests were performed in the direction perpendicular to the bed joint (vertical or y direction) as per the relevant EN standard [27]. The tests were executed in single-wythe running bond specimens, 8 units high and 2 units long for total specimen dimensions equal to $430 \times 470 \times 100$mm^3 (length $\times$ height $\times$ thickness).

These tests were performed monotonically in displacement control, displacement being registered at the jack. Measurements of the deformation of the composite in parallel and laterally to the load direction were recorded using LVDTs attached to the masonry specimens for the determination of the Young's modulus and Poisson's ratio in the elastic range. The post-peak deformation behaviour was measured for the determination of the compressive fracture energy. During the post-peak the displacement registered in the jack closely approximated that of the LVDTs. It was therefore decided to remove the instruments from the specimens to protect them from damage and to rely on the jack measurements alone.

2.1.4. Unit-mortar interface

The properties of the interface between the units and the mortar were investigated through bond-wrench and triplet shear tests. The bond strength tests were executed according to the relevant EN standard for bond-wrench testing [28]. The load was applied through a manually operated jack for the application of a bending moment to the unit-mortar interface. The shear strength of the interface was determined according to the standard for the measurement of the initial shear strength of masonry [29]. Instead of the standard procedure of force-controlled load application, a displacement-controlled load was applied for the registration of the post-peak response, allowing the measurement of the residual shear strength and the calculation of the mode-II fracture energy. The tests were executed at three levels of pre-compression: a) 0.2N/mm^2, 0.6N/mm^2 and 1.0N/mm^2. By fitting the results to a Mohr-Coulomb criterion, the cohesion and friction coefficient were determined.

2.1.5. Repair mortar

A high strength cementitious mortar is used as a repointing material at the bed joints in which reinforcement bars are placed. The mortar mix consists of $50-80$% Portland cement, $20-50$% quartz sand, $1-5$% flue dust from cement clinker production and $1-5$% calcium sulfate. According to the manufacturer's technical specifications, the repair mortar can reach a mean compressive strength of 15N/mm^2 within 2 days and 45N/mm^2 at 28 days.

Repair mortar specimens were produced during the repointing process and tested in three-point bending and compression according to the relevant standards for cement and repair mortar [30,31]. The tests on the repair mortar were executed on $160 \times 40 \times 40$mm^3 prismatic mortar specimens at 28 days, subjected to three-point bending and uniaxial compression.

2.1.6. Helical bars

The strengthening was applied through the installation of stainless steel helical bars. The grade of the stainless steel was ASTM 304. All bars were of a diameter $\varnothing$ of 6mm, sufficiently small to fit in 10mm thick mortar joints. Since the strengthening technique includes the placement of bars both horizontally in the bed joints and diagonally through the body of the masonry, the helical bars were subjected to two types of pull-out tests.

The first set of pull-out tests were executed in cylinders made of the repair mortar, installed in $400 \times 400 \times 250$mm^3 concrete specimens [32]. The concrete cubes were cast in wooden moulds according to the relevant EN standard [33]. The cubes were cured for 28 days, at which point a 30mm diameter hole was drilled at the centre of the cube, with a depth of 150mm. The hole was filled with fresh repair mortar and a helical bar was positioned centrally. The specimens were cured for an additional 28 days before testing.

For the second set of pull-out tests, the bars were placed in pre-drilled pilot holes in masonry triplets, providing an anchorage length of 170mm, or $28.33\varnothing$. This anchorage length roughly corresponds to the length of the bar on either side of a developed crack. Preliminary pull-out tests were executed with different pre-drill diameters for studying the effect of pilot-hole diameter on the bond-slip behaviour: a) with $\varnothing - 2\text{mm} = 4\text{mm}$ and b) with $\varnothing - 1\text{mm} = 5\text{mm}$. The former yielded a bond force of roughly 3kN, while the latter yielded roughly 4kN. This behaviour is in agreement with the trend noted in similar helical bars with a slightly larger diameter but similar anchorage length [34]. Ultimately, the 5mm pilot hole was elected for this set of tests and for application in the wall due to the higher capacity obtained in the preliminary tests.

2.2. Masonry walls

2.2.1. Construction

Two geometrically identical masonry walls were constructed in single-wythe running bond (Fig. 1). This configuration facilitates visual inspection and the highlighting of tensile damage. The full dimensions of the walls were $3070 \times 2690 \times 100$mm^3 (length $\times$ height $\times$ thickness). A single window opening with an area of 780×1510mm^2 (length $\times$ height) was eccentrically included in the walls. A simple concrete lintel was constructed above the window opening. The walls were constructed atop a HEB 300 steel beam and capped with a HEB 600 steel beam, which also provided, along with some additional dead weight, a constant vertical stress of 0.12N/mm^2. The two steel beams were connected with two HEB 300 columns. The steel supporting frame was set in a cantilever configuration, allowing free rotation of the top beam. A high-strength epoxy paste was applied between the masonry and the steel beams to prevent sliding. Each wall was constructed by an experienced mason within a single day. A schematic of the test setup is provided in Fig. 1.

Neither wall was strengthened in its initial state. However, cracking damage typical of soil subsidence was artificially introduced in one of the specimens [35]. This was accomplished through the inclusion of thin plastic sheets between units and mortar during construction for the prevention of the full development of the unit-mortar interface at targeted joints. Soil subsidence induces crack in the masonry, which in traditional brick masonry structures form at the unit-mortar interface due to the poor bond between the two materials. The plastic sheets simulate the effects of subsidence-induced cracks by separating the units from the mortar. The damage simulation does not prevent the curing of the mortar, which is, therefore, able to develop its compressive strength and stiffness. The location of the application of this

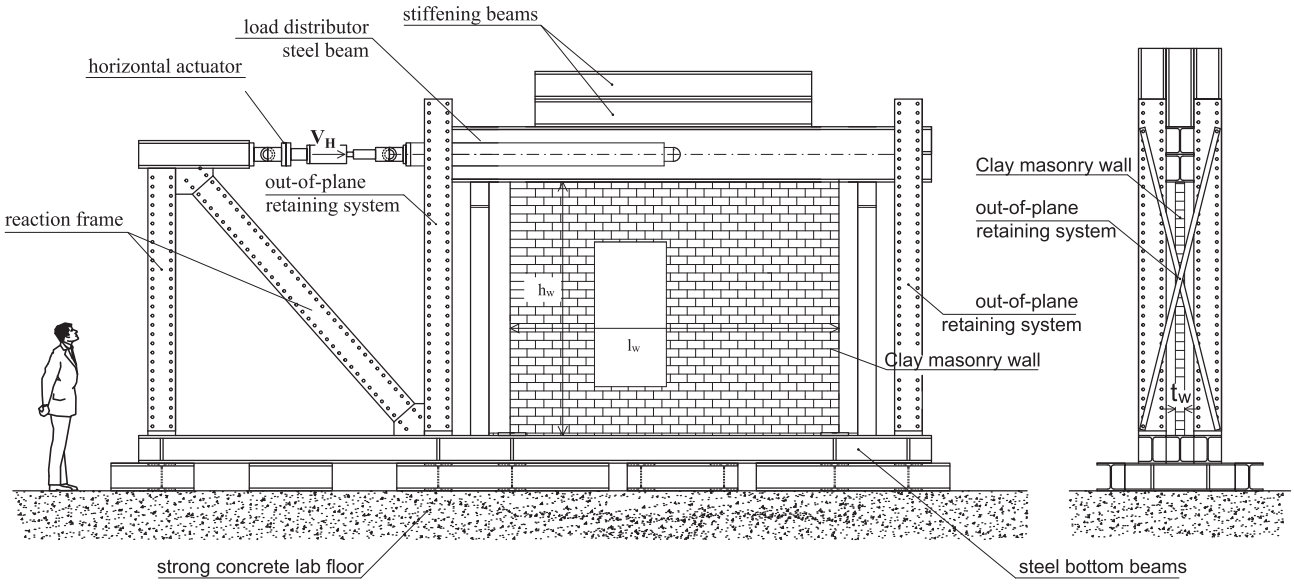

Fig. 1. Test setup for masonry wall in-plane testing.

simulated damage was identified through numerical modelling [36] and consists in diagonal stepped cracks through the mortar joints at the corners of the window opening. These cracks will be referred to as "pre-damage" in this paper.

2.2.2. Testing protocol

Both walls were tested in quasi-static repeated and cyclic loading for the simulation of seismic action, the determination of elastic stiffness and capacity and the evaluation of the failure mode. The loading consists in imposed horizontal deformation applied by an actuator at the top steel beam. This load is controlled by a linear potentiometer measuring the horizontal displacement of the top beam. The net horizontal displacement is defined as the horizontal displacement of the top beam with respect to an external reference point, excluding rotations of the setup and horizontal displacement of the bottom beam with respect to the external reference.

The loading protocol is split in three phases: a) phase 1, consisting in low amplitude repeated loading in the positive direction, b) phase 2, consisting in low amplitude cyclic loading and c) phase 3, consisting in high amplitude cyclic loading. Phases 1 and 2 correspond to the Damage Limitation (DL) state, while phase 3 to the Near Collapse (NC) state. Phase 1 was executed in a repeated rather than a cyclic loading scheme in order to limit stress reversal on the crack surfaces and to highlight crack propagation between cycles. Phases 2 and 3 were executed in a cyclic scheme in order to simulate seismic events of low and high magnitude respectively [36].

The number and relative amplitude of the cycles was determined based on observations on flexure-driven failure mechanisms in building structures [37] located in areas of low seismicity [38]. The relatively low vertical stress in the specimens of the present investigation (roughly 1% of the compressive strength of the masonry composite) was expected to result in a predominantly flexural response, while the seismicity in Groningen is generally low.

The followed testing protocol is detailed in Table 1. The loading protocol is broken down in the three investigated phases, each featuring several cycles. Each cycle encompasses a number of repeated or cyclic applications of net horizontal displacement of a given magnitude. The cumulative number of these applications are referred to as "runs". The loading rate in Phases 1 and 2 was kept sufficiently low to allow clearer crack formation and propagation, while in Phase 3 it was increased proportionally to the target net horizontal displacement. The testing of the unstrengthened wall was stopped during cycle 18, while the strengthened wall reached cycle 20. In both cases the testing was stopped due to extensive damage to the walls.

Table 1
Testing protocol for in-plane shear of masonry walls.

Phase	Cycle	Run		Net horizontal displacement		Loading rate
				mm	mm	mm/s
1	C1	1	30	0.73	–	0.125
	C2	31	60	0.92	–	0.125
	C3	61	90	1.09	–	0.125
	C4	91	120	1.28	–	0.125
	C5	121	150	1.50	–	0.125
2	C6	151	180	0.73	−0.75	0.125
	C7	181	210	0.92	−0.96	0.125
	C8	211	240	1.13	−1.15	0.125
	C9	241	270	1.33	−1.37	0.125
	C10	271	300	1.53	−1.58	0.125
	C11	301	330	1.72	−1.77	0.125
	C12	331	360	1.93	−1.98	0.125
3	C13	361	364	2.48	−2.52	0.036
	C14	365	368	7.87	−7.91	0.108
	C15	369	370	13.28	−13.29	0.180
	C16	371	372	26.76	−26.79	0.360
	C17	373	374	40.25	−40.30	0.540
	C18	375	376	53.77	−53.80	0.720
	C19	377	378	67.26	−67.28	0.900
	C20	379	380	80.76	−63.31	1.080

A speckle pattern was applied on one side of each wall for the monitoring of the in-plane deformation field through single-camera digital image correlation (DIC) [39]. This approach allows the measurement of crack width and length on the surface of the specimens at locations where cracks are expected to propagate, including the areas of pre- and post-damage.

The other side of each wall was fitted with 44 linear potentiometers measuring in-plane vertical, horizontal and diagonal deformations and crack propagation. Additionally, 4 laser sensors were used for measuring the out-of-plane deformation of the two piers and the top beam. The instrumentation is illustrated in Fig. 2. The linear potentiometers were used to measure the vertical displacement of the top beam and wall with respect to the bottom beam, the horizontal displacement .of the top and bottom beams with respect to an external reference, the horizontal sliding and vertical displacement between selected rows of bricks, the diagonal deformation of the wall and the opening of cracks.

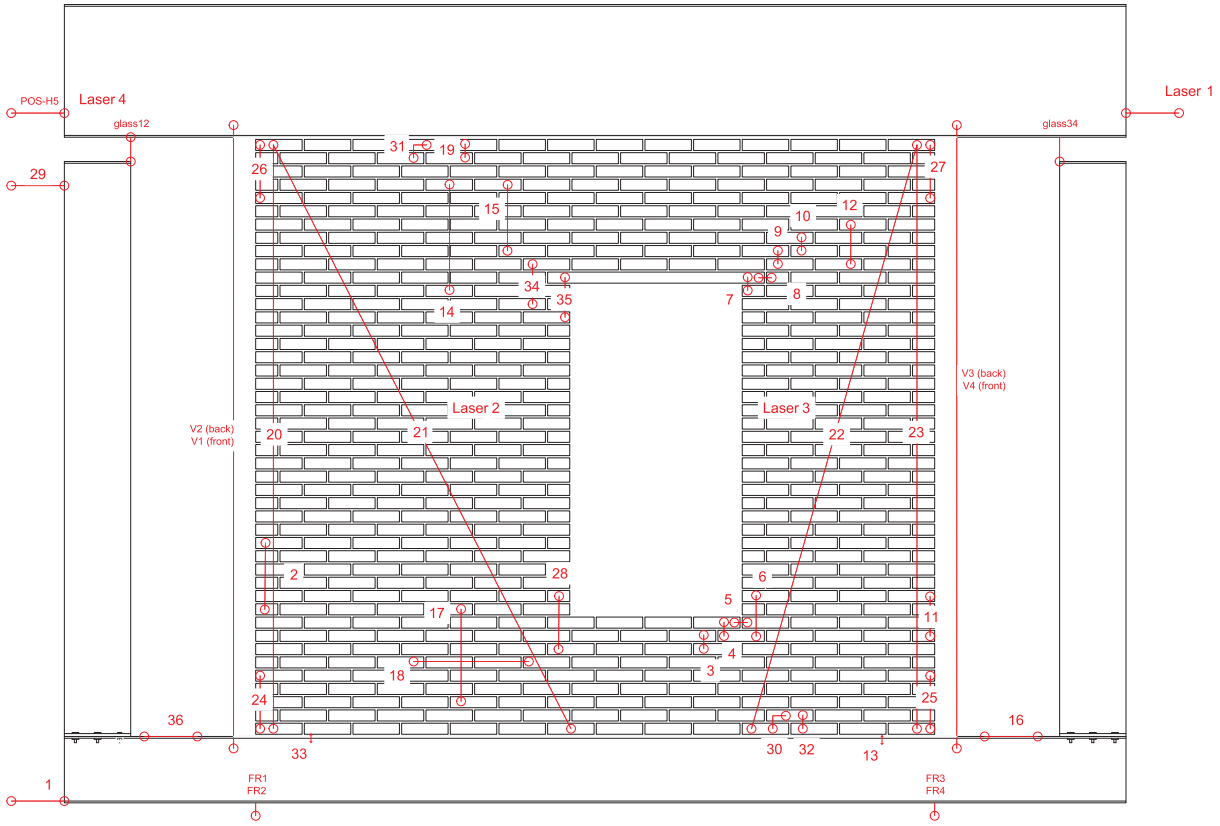

Fig. 2. Sensor layout at the back of the masonry wall for in-plane testing. Placement locations of linear potentiometers and laser sensor targets indicated.

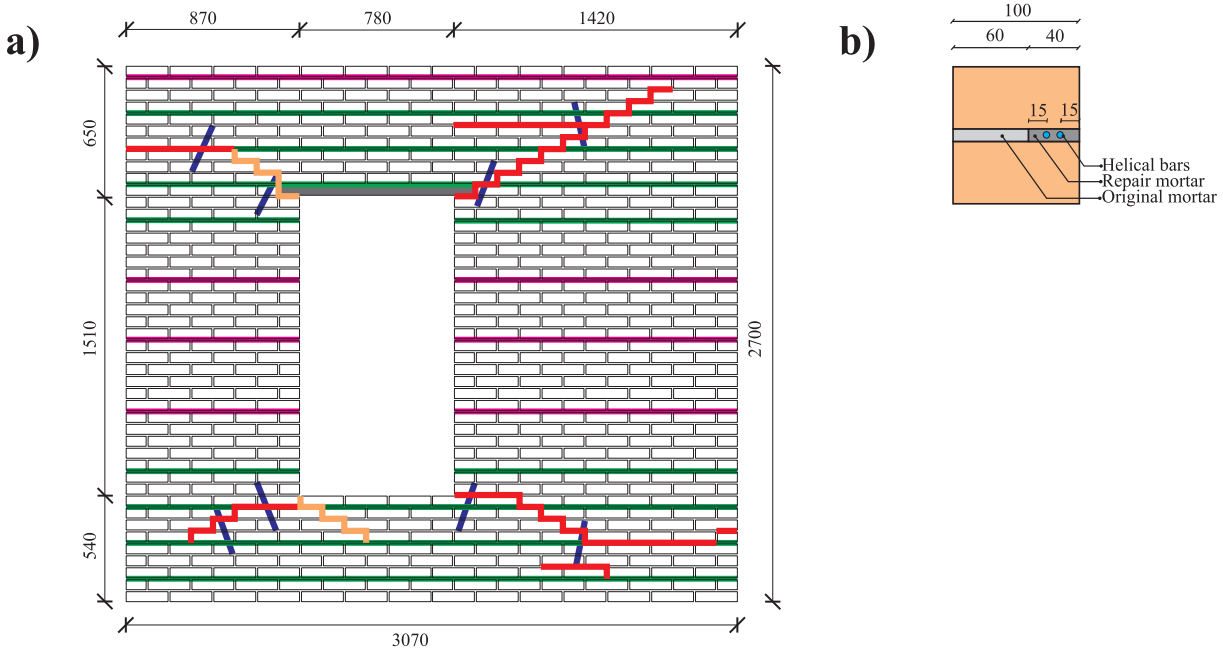

Fig. 3. a) Wall geometry, pre- and post-damage locations and strengthening layout: pre-damage in orange, post-damage in red, double bed joint bars in green, single bed joint bars in purple and single diagonal bars in blue. Positive loading direction towards right. b) Cross-section of repointed bed joint. All dimensions in **mm**.

2.2.3. Strengthening

The wall with simulated pre-damage underwent a strengthening intervention at the end of phase 2, after which the entire loading protocol was restarted. The intervention consisted in a) the embedment of the helical bars in the horizontal bed joints and b) the placement of diagonal bars across cracks formed by in-plane loading. The bed joint reinforcement was placed in repointed mortar joints. The repointing process itself consisted in the cutting of 4 cm deep grooves in the bed joints, the injection of a repointing layer of repair mortar, the placement of the helical bars individually or in pairs and the filling of the remaining joint with a further layer of injected repair mortar. The final repointing layer consists in a thin application of regular mortar for maintaining aesthetic consistency with the existing joints. Above and below the window opening the bars were placed in pairs every 3 joints.

The bar pairs were not mechanically joined or welded. The piers were strengthened with a single bar every 5 or 6 joints. The diagonal bars are installed in 5mm pilot holes, drilled from the external face of the wall across its thickness. The wall in which no bars were installed will be referred to as “unstrengthened” and the wall in which the bars were installed will be referred to as “strengthened”.

The bed joint reinforcement bars extend through undamaged and damaged mortar joints alike. The damage caused by mechanical loading prior to strengthening will be referred to as “post-damage” in this paper. The joints that feature neither pre- or post-damage and that were not located in reinforced regions will be referred to as “virgin joints”. Joints that were strengthened without having suffered damage will be referred to as “strengthened”, while joints having suffered either pre- or post-damage and having subsequently been strengthened will be referred to as “repaired” joints.

The strengthening was undertaken by a construction crew experienced in the application of the technique in practice. The layout and number of reinforcement bars were consistent with application practices in the field. Due to the small thickness of the single-wythe wall, the bed joints reinforcement was installed single-sided, meaning that the bars were placed roughly 20mm eccentrically to the centre of the 100mm-thick wall (Fig. 3b).

A drawing of the wall, including pre- and post-damage and strengthening layout is shown in Fig. 3a. The slender pier on the left of the figure, with a length of 870mm, will be referred to as “Pier 1”, while the pier on the right, with a length of 1420mm, will be referred to as “Pier 2”.

3. Wall test results

3.1. Comparison of unstrengthened and strengthened walls

The results of the in-plane shear tests for the walls are presented in terms of force–displacement graphs and crack patterns for each loading phase and separately for the unstrengthened and strengthened wall configuration.

The results of phase 1 are illustrated in Fig. 4. The displacement envelope, stiffness and peak force are not significantly different between unstrengthened and strengthened walls. However, there is a noticeable reduction in residual displacement at the end of this loading phase, from 0.25mm to 0.15mm. In terms of crack pattern, the unstrengthened wall presents typical diagonal cracks around the window opening (cracks 1 and 2 in Fig. 4c). For the strengthened wall, while crack 1, which includes a pre-damaged area, re-opens, crack 2 shifts to a horizontal crack, caused by bending. The formation of a diagonal crack is prevented from the reinforcement bars in the spandrel.

The results of phase 2 are illustrated in Fig. 5. The unstrengthened wall presents a positive residual displacement of roughly 0.3mm after the last positive loading branch and a positive residual displacement of 0.1mm after the last negative loading branch. Conversely the strengthened wall presents a residual displacement of 0.15mm on the side of the last loading branch at each direction. At the end of this phase, crack 1 propagates similarly in both walls. The newly appeared diagonal cracks 3 and 5 are nearly identical in both walls. Crack 4, also diagonal and at the location of the post-damage in the strengthened wall, has a longer extent in the unstrengthened wall. Overall, according to digital image correlation measurements, a reduction between 20% and 25% was registered in maximum crack width and a reduction between 25% and 56% was registered in maximum crack length.

The results of phase 3 are illustrated in Fig. 6. In the unstrengthened wall the diagonal cracks 1a, 3a and 4a propagated to the edges of the wall. The newly formed cracks 6a and 7a propagated diagonally in the spandrel. Increasing the net horizontal displacement, the residual displacement significantly increased. For the strengthened wall the diagonal cracks 3 and 4 are not lengthened as much as in the unstrengthened wall. The newly formed cracks 8, 9, 10 and 11 are nearly horizontal indicating the action of the bars, restricting the formation of pronounced diagonal cracking. Residual displacement again has a more symmetrical pattern and a smaller magnitude in the strengthened wall compared to the unstrengthened case. The test was stopped during the negative branch of cycle 20 due to excessive damage. Unloading to 0 base shear force resulted in a residual displacement of roughly 50mm. The strengthened wall is able to reach a maximum displacement nearly twice that attained by the unstrengthened wall.

The out-of-plane displacements at the centre of the piers were measured during testing. No noticeable out-of-plane displacement was registered in the walls during phases 1 and 2. The out-of-plane displacement of the piers during phase 3 is presented in Fig. 7 in comparison with the in-plane net horizontal displacement. The out-of-plane displacement in the unstrengthened wall at peak in-plane base shear was roughly 2.5mm. The out-of-plane displacement following the onset of extensive damage tended to shift signs, from negative to positive. The residual out-of-plane displacement for both piers was positive at the end of the test. Conversely, the out-of-plane displacement in the strengthened wall at the in-plane displacement corresponding to the peak base shear was 6.0mm and reached a value of 12.5mm for the maximum positive in-plane displacement applied. For the maximum negative in-plane displacement applied, at which point excessive damage had been registered in the wall, the out-of-plane displacement exceeded 30mm towards the negative direction in both piers. Overall, there was a noted accumulation of out-of-plane displacement towards the negative out-of-plane direction, corresponding to the unreinforced side of the wall. This is due to the lower stiffness of the unreinforced side compared to the side repointed with the repair mortar. Pier 1 exhibited overall larger out-of-plane displacement in both walls.

Despite the fact that the walls were constructed and tested under the same conditions, their out-of-plane response under in-plane loading presented significant differences. In particular, the marked increase in the magnitude of the out-of-plane displacements in the strengthened wall compared to the unstrengthened one, in addition to the clear accumulation of displacements in the former case, indicate that the effect of the strengthening on out-of-plane displacements is substantial.

The increase in the out-of-plane displacement of the strengthened wall compared to the unstrengthened configuration is significant and can lead to a reduction of the force capacity of a pier due to induced eccentricity. In Eurocode 6 [40] an equation is proposed for calculating the reduction of the compressive strength of masonry piers due to eccentricity of the applied compressive load. The reduction factor reads:

$$\Phi = 1 - 2\frac{e}{t} \tag{1}$$

where e is the eccentricity and t is the thickness of the pier. Based on this expression, and due to the prevalence of compression effects in rocking piers, a potential reduction of up to 8% may be registered in the calculated capacity of the wall at 20mm in-plane displacement, where the peak force is attained in the experiments.

3.2. Assessment of the strengthening method

The strengthening method is shown to be effective in restoring, and even slightly enhancing, the stiffness and force capacity of the wall after sustaining light damage. The ductility factor of the wall, already very high due to the predominance of rocking in the response of the piers, was enhanced to a higher degree. Interestingly, the strengthening greatly reduces the difference in stiffness, ductility and capacity in the two loading directions (positive and negative). To compare the performance of the unstrengthened and strengthened wall in the framework of seismic assessment, the equivalent bilinear curves [41] were calculated and the main parameters are reported in Table 2.

Significant differences are obtained in the failure mode between the unstrengthened and strengthened wall, with diagonal cracking in the former being more pronounced while the latter developed mostly

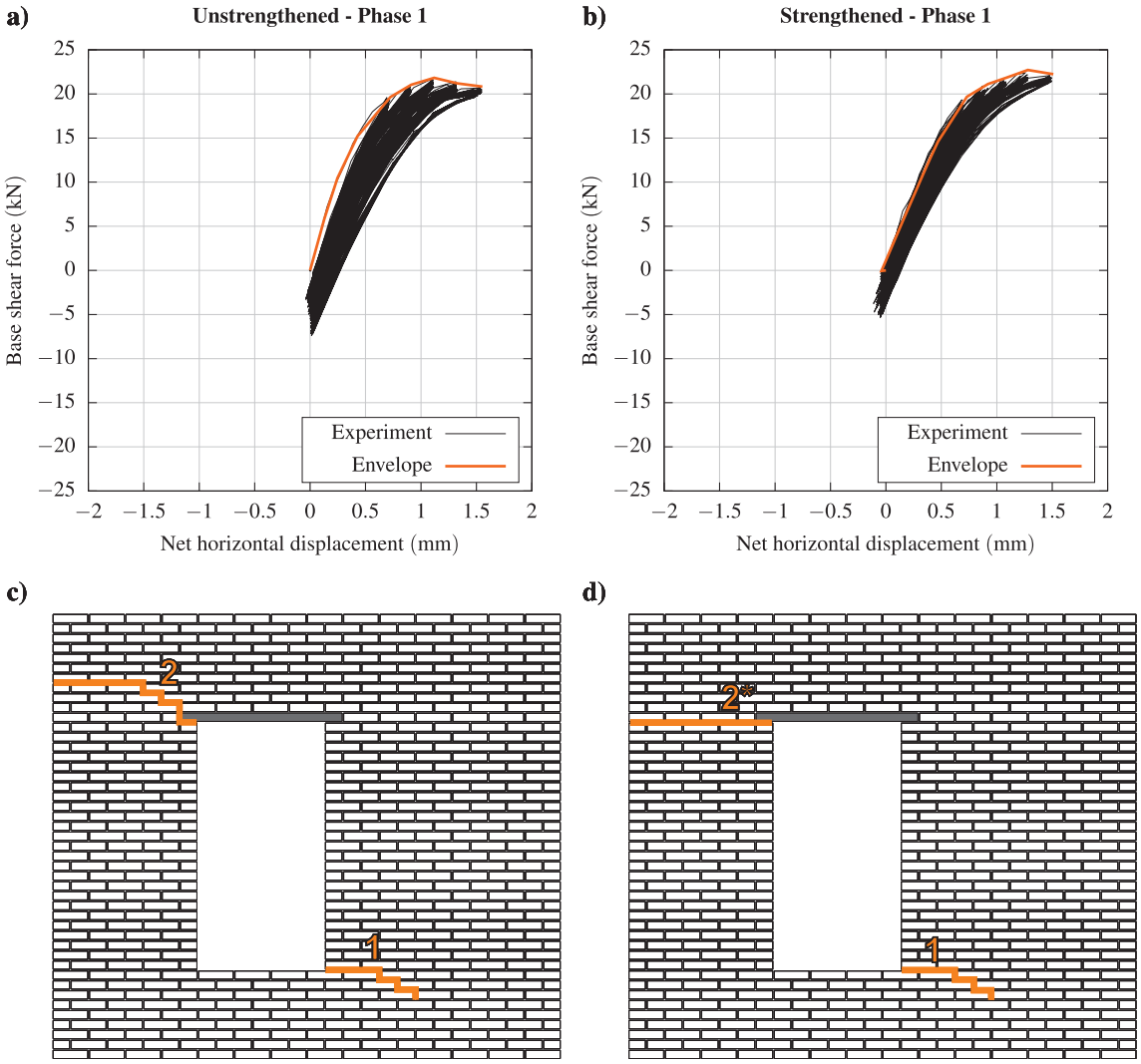

Fig. 4. Experimental results from phase 1: a) force-displacement graph of unstrengthened wall, b) force-displacement graph of strengthened wall, c) crack pattern of unstrengthened wall and d) crack pattern of strengthened wall.

horizontal (rocking) cracks. The containment of diagonal cracking in the spandrel by the reinforcement bars is evident. The increase in force capacity of the walls appears to be the result of this containment, which enhances the frame action of the pier-spandrel system of the wall. The increase in force capacity cannot be attributed to an increase in compressive strength of masonry due to the application of the repair mortar since the virgin and damaged bed joints maintain their original compressive strength. The increase in ductility can be attributed to the contribution of the bars in reducing diagonal cracking in the spandrel, thus maintaining its structural integrity and its capacity for providing frame action between the two piers.

Evidence of strong adhesion of the repair mortar to the clay units was abundant after failure of the joints in the form of broken clay layers attached to intact pieces of mortar. This cannot be considered favourable from a conservation engineering perspective, which promotes compatible and reversible interventions.

The introduction of out-of-plane effects arising from in-plane loading due to the one-sided application of the strengthening raises some minor concerns. Given the noted in-plane character of the response of masonry panels in Groningen [13], the strengthening scheme may introduce out-of-plane effects in cases where none should normally arise. This is potentially detrimental to the strength and durability of traditional brick masonry structures in Groningen.

4. Numerical modelling strategy

The experimental test on the strengthened masonry wall was simulated using non-linear finite element analysis. The purpose of the numerical investigation is to assist the interpretation of the experimental results, including for the calculation of parameters that were not experimentally measured, such as reinforcement bond-slip.

The physical non-linearity of the materials was modelled using an orthotropic continuum smeared crack model [42] implemented in the finite element program DIANA FEA [43]. The analyses were executed under plane-stress assumptions, supplemented by an investigation of out-of-plane effects in 3D elasticity using layered shell elements. Layered shell elements are subdivided across their thickness in two or more layers with different material property assignments. The significance of this approach becomes apparent when studying the structural behaviour of the repointed bed joints.

A meso-modelling approach, in which the units and the mortar are modelled individually, was adopted in this investigation. This approach allows a high level of geometrical fidelity, allowing the direct geometrical representation of all features and the straightforward definitions of the areas of pre- and post-damage. Consequently, it allows for the direct assignment of material properties to each structural component. The number of material parameters is rather high, but these parameters were determined in the investigation of the constituent materials and

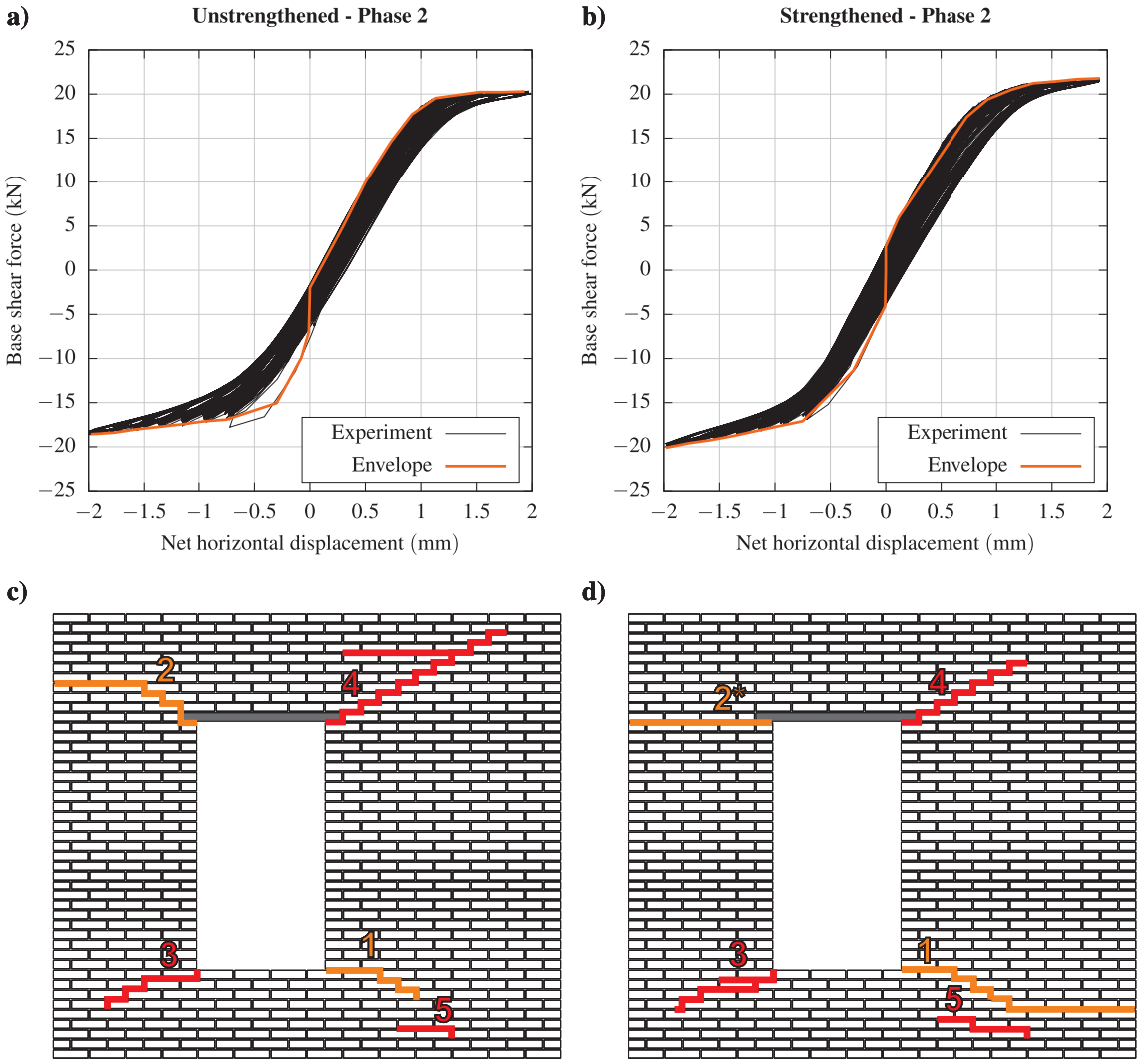

Fig. 5. Experimental results from phase 2: a) force-displacement graph of unstrengthened wall, b) force-displacement graph of strengthened wall, c) crack pattern of unstrengthened wall and d) crack pattern of strengthened wall.

the unit-mortar interface.

The masonry is modelled using plane stress continuum elements. The bricks are kept linear elastic, since cracking was not observed in the bricks until the last cycle of the experimental testing. Each subdomain was assigned the material properties indicated in Table 3. These properties were directly determined through the companion experimental testing or through limited numerical calibration conducted in this investigation and in a numerical investigation of the unstrengthened walls [36]. The steel beams were modelled as linear elastic beam elements. The edge length of the finite elements was kept constant at 10mm (equal to the thickness of the mortar joints) resulting in a mesh consisting of 71,419 elements.

The obtained pull-out test stress-slip curves were fitted to the bond-slip model proposed in the CEB-FIB Model Code 2010 [44]. The model consists in expressing the shear bond stress τ_0 as a piecewise function of the slip s. The function reads in the notation of the Model Code:

$$\tau_0(s) = \begin{cases} \tau_{max}(s/s_1)^a & \text{for} \quad 0 \le s \le s_1 \\ \tau_{max} & \text{for} \quad s_1 \le s \le s_2 \\ \tau_{max} - (\tau_{max} - \tau_f)(s - s_2)/(s_3 - s_2) & \text{for} \quad s_2 \le s \le s_3 \\ \tau_f & \text{for} \quad s_3 \le s \end{cases} \tag{2}$$

The function describes a continuous curve with an exponential first part, a horizontal peak stress plateau, a linear softening part and a horizontal residual plateau (Fig. 8). τ_{max} is the peak stress, τ_f is the residual stress, s_1 is the slip at which peak stress is attained, s_2 is the slip until which peak stress is maintained, s_3 is the slip for which the residual stress is reached and a is a numerical parameter in the range [0, 1] controlling the shape of the initial exponential curve until slip s_1.

Based on the experimental results, the experimentally-fitted numerical parameters for the bond-slip model for reinforcement bars embedded in the horizontal bed joints and diagonally in the masonry are presented in Table 4.

Following the application of the self-weight and vertical load, the repeated and cyclic loading protocols of phases 1, 2 and 3 (Table 1) was applied in terms of horizontal displacement on the top beam with a single execution of each repeated or cyclic branch.

The reinforcement bars are modelled as truss elements embedded in the continuum elements. All bars are assigned a uniaxial stress–strain law for modelling potential yielding in tension. Through the introduction of interface elements between the trusses and the masonry continuum, and the assignment of a bond-slip constitutive relation, the pull-out behaviour of the horizontal and diagonal bars can be modelled. The bars are assigned the material properties indicated in Table 3.

Damaged mortar joints, whether of the pre- or post-damage variety, were assigned modified mechanical properties compared to the virgin mortar joints: a) the Young's modulus was reduced by 50%, b) the tensile strength and fracture energy were reduced to zero, c) the friction

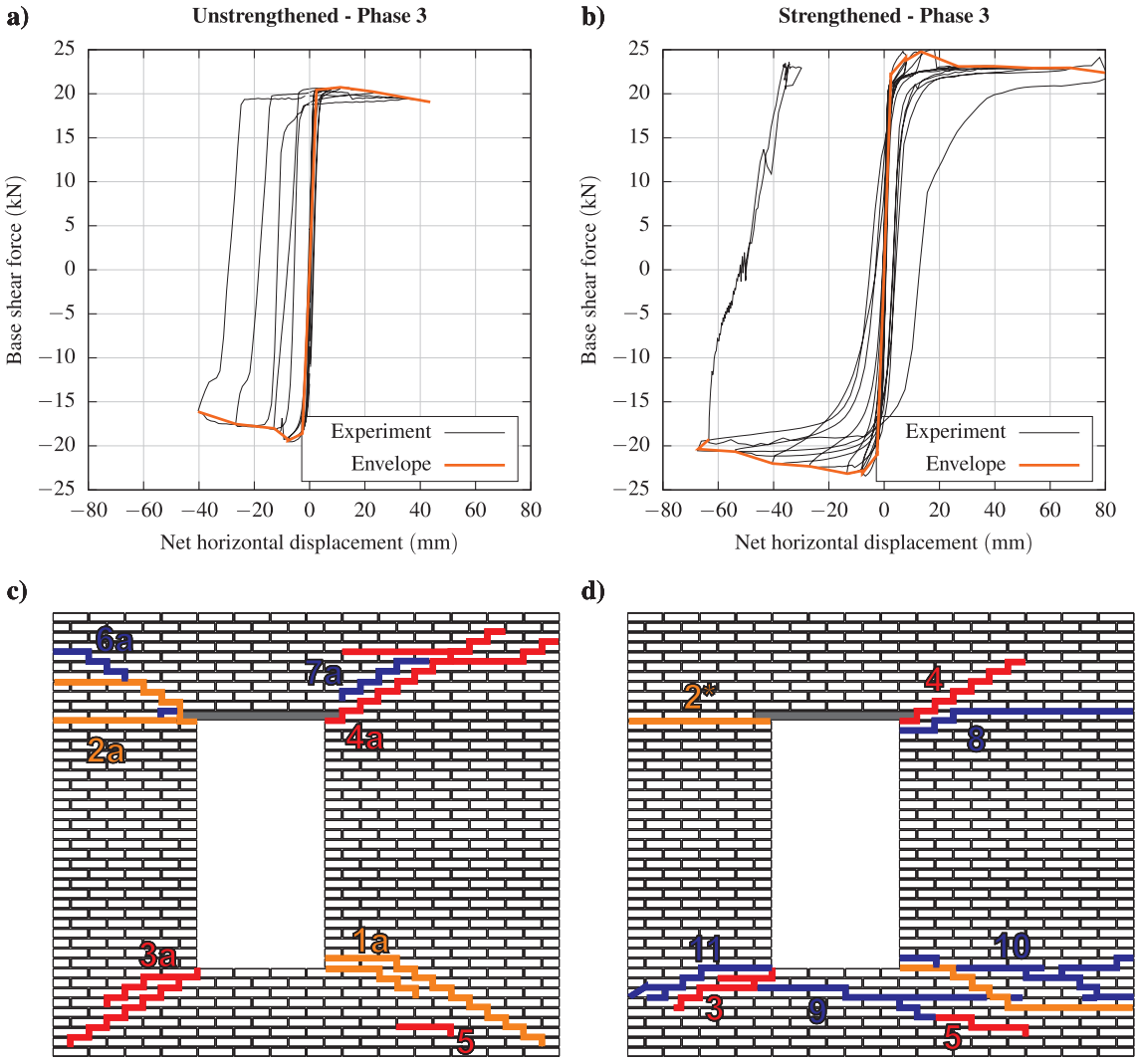

Fig. 6. Experimental results from phase 3: a) force-displacement graph of unstrengthened wall, b) force-displacement graph of strengthened wall, c) crack pattern of unstrengthened wall and d) crack pattern of strengthened wall.

coefficient and cohesion were assigned their residual values and d) the shear fracture energy was reduced to zero. The compressive strength was not reduced. The strategy for the reduction of the strength of the damaged joints was motivated by the observed damage in the wall, which consisted of cracks at the unit-mortar interface with no signs of extensive crushing at the compressed toe. Similarly, and on top of the reduction due to damage, the Young's modulus of all head joints in the meso-model was reduced by 50% for simulating the imperfect compaction of the mortar. This approach was adopted from a previous numerical investigation, in which the meso-model approach was calibrated on similar unstrengthened walls [36].

The strengthening technique introduces changes in the material composition of the mortar joints along the thickness of the masonry. This may be indirectly considered in the plane-stress meso-model. Strengthened joints consist of a layer of virgin mortar 6 cm wide and a layer of repair mortar 4 cm wide. Similarly, repaired joints consist of a layer of damaged mortar 6 cm wide and a layer of repair mortar 4 cm wide. Since the two material phases can be considered to be regularly aligned, similarly to a network of fibres in a composite, a rule of mixtures is applied for the determination of the mechanical properties of the composite joint [45]. Considering a specific material property p, the upper-bound value p_u of this property p_c for a composite material composed of n material phases, each with a property of p_i and a volume fraction equal to f_i, is calculated as:

$$p_c = p_u = \sum_{i=1}^{n} f_i p_i \tag{3}$$

Similarly, the lower-bound value p_l of the same property can be calculated as:

$$p_c = p_l = \left(\sum_{i=1}^{n} \frac{p_i}{f_i} \right)^{-1} \tag{4}$$

According to these two equations and disregarding the contribution of the helical bars for simplicity, one obtains the potential minimum and maximum values for material properties of the strengthened and repaired joints. These values are listed in Table 5. The properties of the unit-repair mortar interface were not experimentally investigated and were assigned the same properties as the unit-mortar interface. According to the calculations, the lower bound approach, which would in principle be more accurate for layers arranged perpendicularly to the load, produces unrealistically low values for the tensile and shear strength and fracture energy. Additionally, adopting the lower-bound Young's modulus results in a deviation of the numerically- from the experimentally-derived stiffness of the wall. Therefore, it was decided to use the upper-bound values for all parameters.

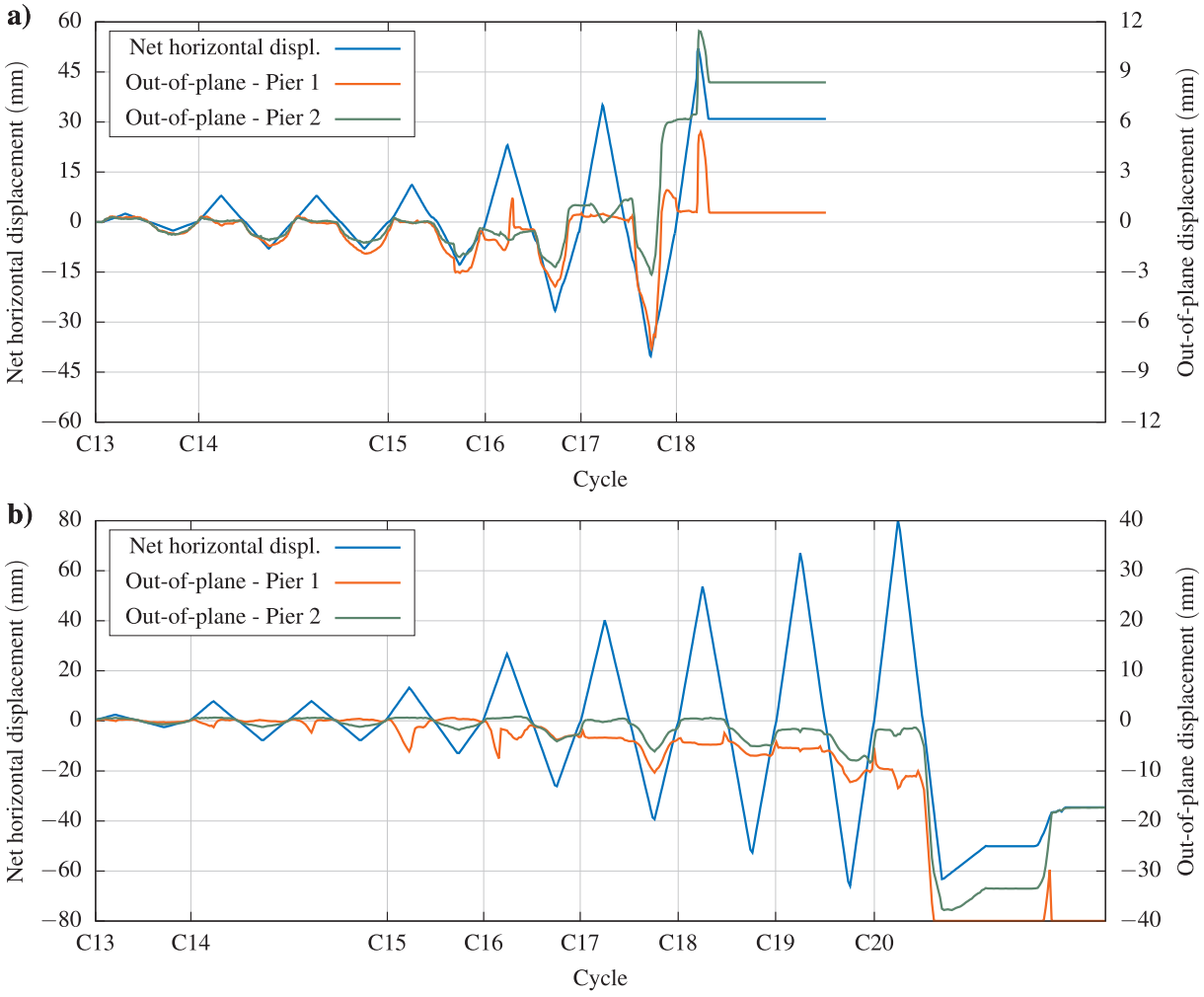

Fig. 7. Time-history of in-plane and of out-of-plane displacement of piers for a) unstrengthened and b) strengthened walls during phase 3.

5. Analysis results

A comparison of the experimental and numerically derived force–displacement curves is shown in Fig. 9. Up to the end of phase 2 the force response of the wall is overestimated in the positive direction but well approximated in the negative. During phase 3 the numerically obtained force response is overestimated in the initial loading branches but converges with the experimentally obtained response for applied displacement greater than 30mm. The unloading branches are generally well simulated up to a displacement of 50mm, particularly in the negative loading direction. The higher energy dissipation in the analysis compared to the experiment can be partly attributed to the influence of out-of-plane deflection, which is disregarded in the present numerical analysis.

The cracking patterns obtained in the strengthened wall at various levels of applied displacement are presented in Fig. 10. The experimentally registered crack patterns have been produced through processing of DIC data. The numerical model is able to reproduce with very good accuracy the experimental crack pattern in the DL phase and up to the peak force. Some differences are noted at the base of pier 1, which exhibits more pronounced cracking in the numerical model. The greater crack propagation length in the model can potentially further contribute to the differences in energy dissipation between the model and the experiment. At maximum applied displacement, the numerical model is able to reproduce the network of cracks below the base of the piers and below the window with reasonable accuracy. Most notably, the model is able to capture the initial opening and subsequent closing of the diagonal crack propagating from the upper right corner of the

Table 2
Parameters of equivalent bilinear curves. Percentile difference due to strengthening in parentheses.

		Unstrengthened		Strengthened	
Parameter	Unit	Negative	Positive	Negative	Positive
Stiffness	kN/mm	22.67	14.22	23.16 (2.2%)	23.76 (67.1%)
Ultimate displacement	mm	−40.3	43.63	−63.30 (57.1%)	80.76 (85.1%)
Maximum base shear	kN	−17.72	20.25	−21.92 (23.7%)	23.19 (14.5%)
Elastic displacement	mm	−0.78	1.42	−0.94 (20.5%)	0.98 (-31.0%)
Ductility factor	–	51.5	30.6	66.9 (29.9%)	82.7 (170.3%)
Ultimate drift	%	−1.49	1.61	−2.34 (57.0%)	2.99 (85.7%)

Table 3
Summary of material parameters.

Material	Parameter	Symbol	Units	Average	Coefficient of variation	No. of specimens	Standard
Units	Compressive strength	$f_{c,u}$	N/mm^2	28.31	0.10	9	EN 772-1
	Young's modulus	E_u	N/mm^2	8049	0.05	2	EN 772-1
	Poisson's ratio	ν_u	–	0.15[a]	–	–	–
	Flexural strength	$f_{b,u}$	N/mm^2	6.31	0.11	8	NEN 6790
	Density	ρ_u	kg/m^3	1708[b]	–	–	–
Construction mortar	Compressive strength	$f_{c,m}$	N/mm^2	3.59	0.09	24	EN 1015-11
	Compressive fracture energy	$G_{c,m}$	N/mm	6.4[a]	–	–	–
	Young's modulus	E_m	N/mm^2	1050[a]	–	–	–
	Poisson's ratio	ν_m	–	0.20[a]	–	–	–
	Flexural strength	$f_{b,m}$	N/mm^2	1.55	0.10	12	EN 1015-11
	Density	ρ_m	kg/m^3	1708[b]	–	–	–
Masonry composite	Vertical compressive strength	$f_{c,cy}$	N/mm^2	12.93	0.07	3	EN 1052-1
	Vertical compressive fracture energy	$G_{c,cy}$	N/mm	28.63	0.12	3	EN 1052-1
	Vertical Young's modulus	$E_{c,x}$	N/mm^2	3207	0.18	3	EN 1052-1
	Density	ρ_m	kg/m^3	1708	0.07	19	–
Unit-mortar interface	Bond strength	$f_{t,i}$	N/mm^2	0.08	0.32	10	EN 1052-5
	Bond fracture energy	$G_{t,i}$	N/mm	0.0069	–	–	–
	Initial shear strength	f_{v0}	N/mm^2	0.13	–	6	EN 1052-3
	Residual shear strength	f_{vr}	N/mm^2	0.04	–	6	EN 1052-3
	Shear fracture energy	$G_{v,i}$	N/mm	0.3	–	–	–
	Initial friction coefficient	μ_0	–	0.82	–	6	EN 1052-3
	Residual friction coefficient	μ_r	–	0.63	–	6	EN 1052-3
Repair mortar	Compressive strength	$f_{c,M}$	N/mm^2	46.62	0.09	18	EN 196-1
	Compressive fracture energy	$G_{c,M}$	N/mm	80[a]	–	–	–
	Young's modulus	E_M	N/mm^2	15000[a]	–	–	–
	Poisson's ratio	ν_M	–	0.20*	–		–
	Flexural strength	$f_{b,M}$	N/mm^2	7.68	0.24	9	EN 196-1
	Density	ρ_M	kg/m^3	1922	0.03	9	EN 196-1
Helical bars	Young's modulus	E_h	N/mm^2	194,000	–	–	–
	Yield strength	$f_{y,h}$	N/mm^2	205	–	–	–
	Tensile strength	$f_{s,h}$	N/mm^2	515	–	–	–

[a] From numerical calibration.
[b] Assigned the value measured for masonry.

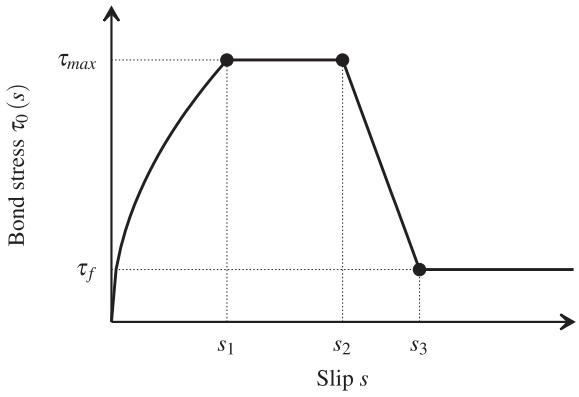

Fig. 8. Reinforcement bar bond-slip curve according to Model Code 2010.

Table 4
Experimentally-fitted parameters for bond-slip model according to Model Code 2010.

	s_1 mm	s_2 mm	s_3 mm	τ_{max} N/mm^2	τ_f N/mm^2	a –
Bed joint	5.0	110.0	120.0	2.0	0.05	0.7
Masonry	20.0	45.0	50.0	1.3	0.05	0.7

window.

The results of the bilinear idealisation of the numerically-derived force–displacement curves is shown in Table 6. An excellent approximation of the experimental response is obtained in the positive direction. However, in the negative direction an underestimation of the ductility and a slight overestimation of the capacity are obtained.

Overall, the analysis results are in reasonable agreement with the experimental data in terms of damage pattern, capacity, stiffness and bilinear idealisation of the response; no undue parameter adjustment was performed due to the availability of several companion material tests.

The behaviour of the reinforcement is evaluated based on the amount of slip and the potential yielding of the bars. The numerical analysis results assist this evaluation in the absence of detailed experimental observation and data.

The highest axial stresses in the reinforcement bars are encountered at the bed joint reinforcement immediately below the window opening. During phase 2, the highest developed stress is 156N/mm^2, which is lower than the yield strength of the stainless steel. A plot of the developed stresses at two bars below the window opening are shown in Fig. 11a. Due to the low stiffness of the bond-slip interface of the diagonal bars, the axial stress in the diagonal bars was limited to roughly 23N/mm^2, which is well below their yielding limit.

Due to their being oriented in parallel with the major horizontal cracks formed in unreinforced bed joints, the bed joint reinforcement did not exhibit slip throughout the analysis. The diagonal bars exhibited a maximum slip of 0.44mm during phase 2 at the lower right of the window and a maximum slip of 6.32mm at the upper right of the window during phase 3. This amount of slip lies within the elastic branch of the bond-slip model as described in Table 1. The bond-slip of the two diagonal bars closest to the top of the window versus the applied displacement is plotted in Fig. 11b.

Table 5
Upper- and lower-bound values for the material properties of the strengthened and repaired joints according to the rule of mixtures.

	Compressive strength $f_{c,m}$ N/mm^2	Compressive fracture energy $G_{c,m}$ N/mm	Tensile strength $f_{t,m}$ N/mm^2	Tensile fracture energy $G_{t,m}$ N/mm	Young's modulus E N/mm^2	Initial shear strength f_{v0} N/mm^2	Friction coefficient μ –	Shear fracture energy $G_{s,m}$ N/mm
Strengthened joints	5.69–20.72	36.94–82.75	0.080	0.0069	1672–6630	0.13	0.82	0.30
Repaired joints	5.69–20.72	36.94–82.75	~0.000–0.032	~0.000–0.003	855–6315	0.02–0.06	0.59–0.63	~0.00–0.12

It is not possible to simulate the out-of-plane effects in structures loaded in-plane through a plane stress approach. These effects can, however, be simulated using layered shell elements. By varying the properties of the bed joints along the thickness in order to consider the single-sided strengthening with repair mortar, out-of-plane strains are introduced in the wall. A full-nonlinear analysis of the layered shell model was not practical due to high computational cost. Therefore, a linear elastic analysis was opted for in this investigation. It is not expected that a linear analysis provide an accurate prediction of the behaviour of the wall, but it can be illustrative of some key characteristics of the response.

For an application of a net horizontal displacement of 1.00mm, a 0.14mm out-of-plane displacement towards the unreinforced side is obtained at the centre-height of pier 2. Multiplying this result by a factor of 20, this result is consistent with the magnitude of out-of-plane displacement measured in the experiments at an applied in-plane displacement of 20mm.

Performing the same three-dimensional finite element analysis assuming a combination of in-situ natural hydraulic lime mortar, assigning a lowered Young's modulus of 250N/mm^2 [46], and the same repair mortar for repointing, the out-of-plane deformation is increased to 0.20mm. It is therefore expected that in actual historic buildings strengthened with this method, the out-of-plane effects would be consistent with this latter, unfavourable result. In combination with potential eccentric loads and imperfections already present, the added eccentricity introduced by the repair mortar may have an even more adverse effect in single-wythe walls. Double-wythe walls, which are frequently encountered in historic buildings and in which the repointing is performed in a smaller percentage of the joint thickness, are potentially less sensitive to these eccentricity effects.

6. Conclusions

A strengthening technique consisting in bed joint reinforced repointing and the placement of diagonal anchors has been investigated. While typically used for the repair of subsidence-induced damage, this technique assumes a new role as a strengthening measure against induced seismicity. Through an experimental and numerical investigation presented in this paper, the technique can be assessed on multiple levels.

In terms of applicability, the strengthening is quick to apply and has a limited impact on building aesthetic. The repair mortar sets very quickly, providing strength and stability nearly immediately after application. The disturbance to the masonry from cutting grooves in the bed joints and drilling diagonal pilot holes in the masonry is limited due to the softness of the bed joint mortar and the small diameter required for the diagonal bars.

The strengthening provided a modest increase of the stiffness and maximum base shear force of the wall tested under quasi-static repeated and cyclic loading. Further, it resulted in a more even response in the two loading directions compared to the unstrengthened case. The cracking pattern shifts from mostly diagonal cracks in the spandrel and base to mostly horizontal cracks below the piers. Ultimately, for displacements 53.7% larger than the ultimate displacement of the unstrengthened wall, the strengthened wall showed formation of toe-crushing and substantial out-of-plane deformations; the latter related to the asymmetric positions of the bars and the repair mortar within the thickness of the wall.

The evaluation of the behaviour of the bars through numerical analysis revealed that the bed joint bars below the window opening develop high axial stresses, without reaching yielding, which additionally cause the formation of a network of horizontal cracks in the

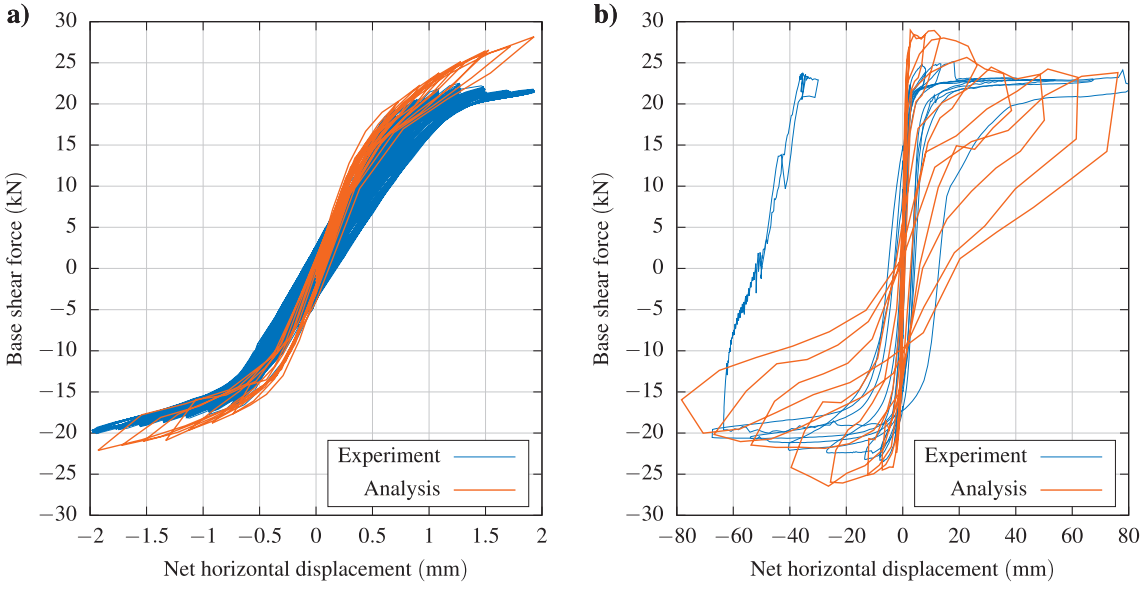

Fig. 9. Comparison of experimental and numerical force-displacement curves for a) phases 1 and 2, b) phase3.

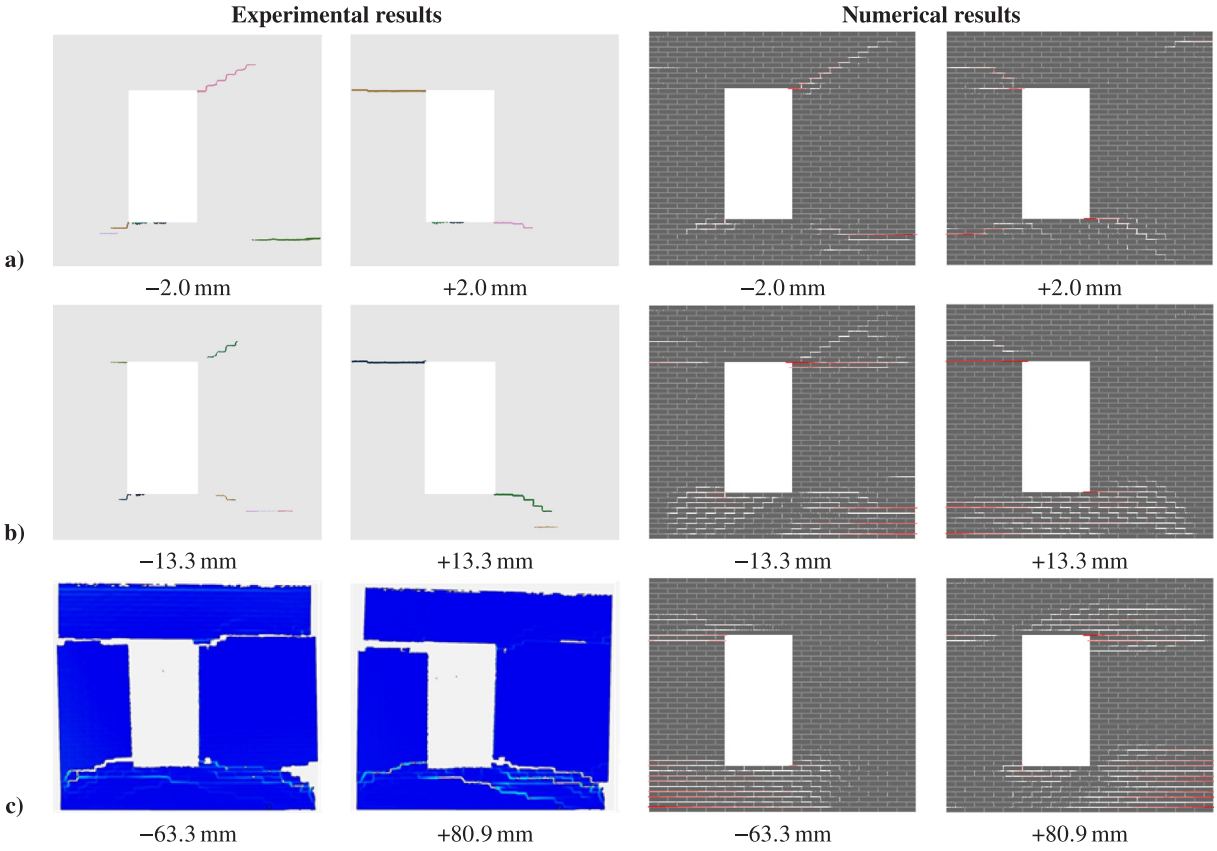

Fig. 10. Comparison of experimentally and numerically obtained (open cracks in red, closed cracks in white) cracking patterns for different levels of applied displacement: a) at the end of phase 2, b) near peak force and c) at the maximum applied displacement.

Table 6
Bilinear approximation parameters for numerical capacity curves. Percentile difference from experimentally-derived bilinear approximation in parentheses.

Parameter	Unit	Negative	Positive
Stiffness	kN/mm	18.41 (−20.5%)	24.98 (5.1%)
Ultimate displacement	mm	−54.44 (−16.3%)	80.76 (0.0%)
Maximum base shear	kN	24.54 (10.7%)	25.27 (8.2%)
Elastic displacement	mm	1.33 (29.3%)	1.01 (3.0%)
Ductility factor	–	40.84 (−38.9%)	79.79 (−3.6%)
Ultimate drift	%	−2.02 (−15.8%)	2.99 (0.0%)

unstrengthened bed joints. Substantial bond-slip is registered in the diagonal bars above the window. Nevertheless, the strengthening layout can be considered effective in prohibiting the re-opening of large diagonal cracks in the spandrels, similarly to the bed joint reinforcement.

The high strength and stiffness of the repair mortar raised concerns for the compatibility of the technique when applied to single-wythe walls. Out-of-plane effects were registered in the experiments, as predicted through analytical modelling of the properties of the reinforced bed joints. These effects, while not critical in the case of seismic events, which typically induce combined in- and out-of-plane forces, can be detrimental to the resilience and capacity of masonry members. Given that the compressive strength of the joints is secondary for the capacity of rocking piers under low levels of vertical stress, and given that bond-slip of bed joint bars is unlikely as shown in the numerical results, the necessity of such a strong and stiff repair mortar is questioned. Other issues, stemming from chemical compatibility and conservation engineering principles, need to be considered in future applications in historic buildings.

Overall, the strengthening technique, is shown to be an effective intervention method for both low- and high-magnitude seismicity. However, the use of a lower strength repointing mortar is advised for application in historic buildings. The effectiveness of the technique in the field needs to be verified through site inspection of strengthened buildings in the Region of Groningen. This next step of investigation is currently underway, along with the experimental investigation of the technique using a lower strength repointing mortar. Finally, an investigation on the effect of an increased anchorage length of the diagonal bars is recommended, with due consideration to construction difficulties and conservation engineering principle.

CRediT authorship contribution statement

Anastasios Drougkas: Conceptualization, Methodology, Writing - original draft. **Lucia Licciardello:** Investigation, Data curation, Writing - original draft. **Jan G. Rots:** Funding acquisition, Writing - review & editing. **Rita Esposito:** Supervision, Funding acquisition, Project administration, Writing - review & editing.

Declaration of Competing Interest

The authors declare that they have no known competing financial interests or personal relationships that could have appeared to influence the work reported in this paper.

Acknowledgements

This research was funded by the Rijksdienst voor het Cultureel Erfgoed (RCE), part of the Ministerie van Onderwijs, Cultuur en Wetenschap (OCW), the Netherlands, subsidy No. MS-2018-189, which is gratefully acknowledged.

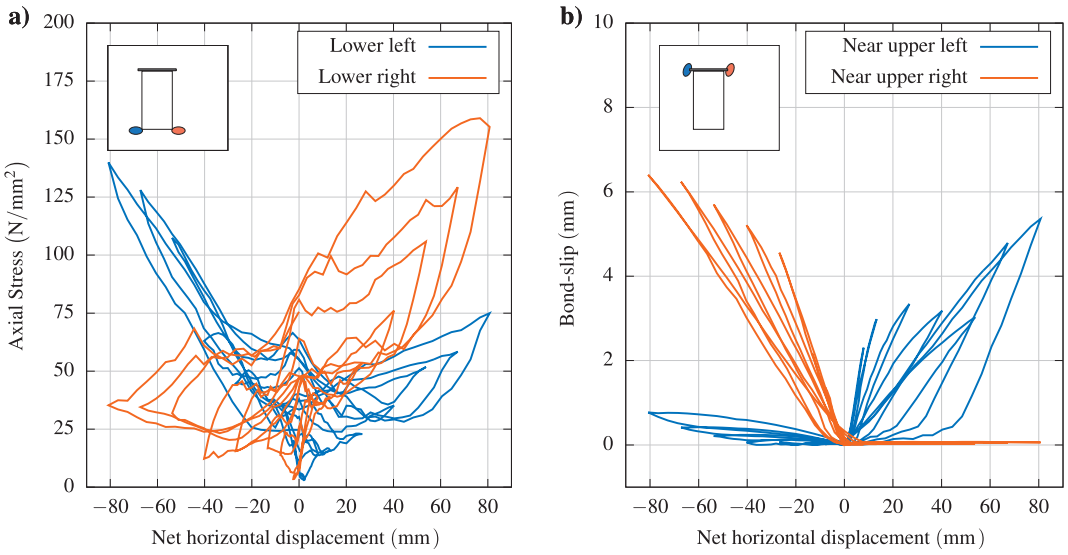

Fig. 11. Performance of reinforcement bars during phase 3: a) axial stress of bed joint bars near the base of the window, b) bond-slip of diagonal bars near the top of the window. Locations of measurements indicated in wall drawing insets.

References

[1] Foulger GR, Wilson MP, Gluyas JG, Julian BR, Davies RJ. Global review of human-induced earthquakes. Earth-Science Rev 2018;178:438–514. https://doi.org/10.1016/j.earscirev.2017.07.008.

[2] Vlek C. Induced Earthquakes from Long-Term Gas Extraction in Groningen, the Netherlands: Statistical Analysis and Prognosis for Acceptable-Risk Regulation. Risk Anal 2018;38. https://doi.org/10.1111/risa.12967.

[3] Son M, Cording EJ. Evaluation of Building Stiffness for Building Response Analysis to Excavation-Induced Ground Movements. J Geotech Geoenvironmental Eng 2007;133:995–1002. https://doi.org/10.1061/(ASCE)1090-0241(2007)133:8(995).

[4] Morandi P, Albanesi L, Graziotti F, Li Piani T, Penna A, Magenes G. Development of a dataset on the in-plane experimental response of URM piers with bricks and blocks. Constr Build Mater 2018;190:593–611. https://doi.org/10.1016/j.conbuildmat.2018.09.070.

[5] Penna A, Morandi P, Rota M, Manzini CF, Da Porto F, Magenes G. Performance of masonry buildings during the Emilia 2012 earthquake. Bull Earthq Eng 2013;12. https://doi.org/10.1007/s10518-013-9496-6.

[6] Giardina G, Hendriks MAN, Rots JG. Sensitivity study on tunnelling induced damage to a masonry façade. Eng Struct 2015;89. https://doi.org/10.1016/j.engstruct.2015.01.042.

[7] Drougkas A, Roca P, Molins C. Experimental Analysis and Detailed Micro-Modeling of Masonry Walls Subjected to In-Plane Shear. Eng Fail Anal 2019;95:82–95. https://doi.org/10.1016/j.engfailanal.2018.08.030.

[8] Parisi F, Augenti N, Prota A. Implications of the spandrel type on the lateral behavior of unreinforced masonry walls. Earthq Eng Struct Dyn 2014;43. https://doi.org/10.1002/eqe.2441.

[9] Foraboschi P. Coupling effect between masonry spandrels and piers. Mater Struct Constr 2009;42:279–300. https://doi.org/10.1617/s11527-008-9405-7.

[10] Drougkas A, Verstrynge E, Szekér P, Heirman G, Bejarano-Urrego L-E, Giardina G, et al. Numerical Modeling of a Church Nave Wall Subjected to Differential Settlements: Soil-Structure Interaction, Time-Dependence and Sensitivity Analysis. Int J Archit Herit 2020. https://doi.org/10.1080/15583058.2019.1602682.

[11] Giardina G, DeJong MJ, Chalmers B, Ormond B, Mair RJ. A comparison of current analytical methods for predicting soil-structure interaction due to tunnelling. Tunn Undergr Sp Technol 2018;79. https://doi.org/10.1016/j.tust.2018.04.013.

[12] Yiu WN, Burd HJ, Martin CM. Finite-element modelling for the assessment of tunnel-induced damage to a masonry building. Géotechnique 2017;67. https://doi.org/10.1680/jgeot.sip17.P.249.

[13] Van Staalduinen P, Terwel K, Rots J. Onderzoek naar de oorzaken van bouwkundige schade in Groningen Methodologie en case studies ter duiding van de oorzaken. Report number: CM-2018-01. TU Delft; 2018.

[14] Petersen RB, Masia MJ, Seracino R. In-Plane Shear Behavior of Masonry Panels Strengthened with NSM CFRP Strips. I: Experimental Investigation. J Compos Constr 2010;14.

[15] Ismail N, Petersen RB, Masia MJ, Ingham JM. Diagonal shear behaviour of unreinforced masonry wallettes strengthened using twisted steel bars. Constr Build Mater 2011;25. https://doi.org/10.1016/j.conbuildmat.2011.04.063.

[16] Haach VG, Vasconcelos G, Lourenço PB. Parametrical study of masonry walls subjected to in-plane loading through numerical modeling. Eng Struct 2011;33. https://doi.org/10.1016/j.engstruct.2011.01.015.

[17] Licciardelo L, Rots JG, Esposito R. Performance of unreinforced masonry strengthened with bed joint reinforced repointing. 12th Int Conf Struct Anal Hist Constr 2021.

[18] Licciardelo L, Rots JG, Esposito R. Experimental tests on masonry strengthened with bed joint reinforced repointing. Heron 2020.

[19] Drougkas A, Licciardelo L, Rots JG, Esposito R. Experimental Testing and Numerical Analysis of Strengthened Historic Masonry Subjected to Induced Seismicity. Greece: XI Int. Conf. Struct. Dyn. Athens; 2020.

[20] Kallioras S, Guerrini G, Tomassetti U, Marchesi B, Penna A, Graziotti F, et al. Experimental seismic performance of a full-scale unreinforced clay-masonry building with flexible timber diaphragms. Eng Struct 2018;161:231–49. https://doi.org/10.1016/j.engstruct.2018.02.016.

[21] Licciardelo L, Esposito R. Experimental study on unreinforced masonry strengthened with bed joint reinforcement. Report number: CM1B07-2. TU Delft; 2019.

[22] CEN. EN 772-1 - Methods of test for masonry units. - Part 1: Determination of compressive strength. 2011.

[23] Nederlands Normalisatie-instituut. NEN 6790 - Technische grondslagen voor bouwconstructies - TGB 1990 - Steenconstructies - Basiseisen en bepalingsmethoden. 2005.

[24] Vermeltfoort A, Martens DRW, van Zijl G. Brick–mortar interface effects on masonry under compression. Can J Civ Eng 2007;34. https://doi.org/10.1139/L07-067.

[25] ASTM. ASTM C 270 - Standard Specification for Mortar for Unit Masonry. 2019.

[26] CEN. EN 1015-11 - Methods of test for mortar for masonry - Part 11: Determination of flexural and compressive strength of hardened mortar. 2007.

[27] CEN. EN 1052-1 - Methods of test for masonry - Part 1: Determination of compressive strength. 1999.

[28] CEN. EN 1052-5 - Methods of test for masonry - Determination of bond strength by the bond wrench method. 2005.

[29] CEN. EN 1052-3 - Methods of test for masonry - Part 3: Determination of initial shear strength. 2002.

[30] CEN. EN 12190 - Products and systems for the protection and repair of concrete structures. Test methods. Determination of compressive strength of repair mortar. 2018.

[31] CEN. EN-196-1 - Methods of testing cement - Part 1: Determination of strength. 2005.

[32] CEN. EN 1881 - Products and systems for the protection and repair of concrete structures. Test methods. Testing of anchoring products by the pull-out method. 2018.

[33] CEN. EN 1766 - Products and systems for the protection and repair of concrete structures. Test methods. Reference concretes for testing. 2017.

[34] Moreira S, Ramos LF, Csikai B, Bastos P. Bond behaviour of twisted stainless steel bars in mortar joints. 9th Int Mason Conf Guimarães 2014:1–8.

[35] Korswagen PA, Longo M, Meulman E, Rots JG. Experimental and computational study of the influence of pre-damage patterns in unreinforced masonry crack propagation due to induced, repeated earthquakes. 13th North Am. Mason. Conf. Salt Lake City, 2019.

[36] Korswagen PA, Longo M, Meulman E, Rots JG. Crack initiation and propagation in unreinforced masonry specimens subjected to repeated in-plane loading during light damage. Bull Earthq Eng 2019;17. https://doi.org/10.1007/s10518-018-00553-5.

[37] Mergos PE, Beyer K. Loading protocols for structures designed for different behaviour factors. SECED 2015 Conf. Earthq. Risk Eng. Towar. a Resilient World, Cambridge, 2015.

[38] Mergos PE, Beyer K. Loading protocols for European regions of low to moderate seismicity. Bull Earthq Eng 2014;12. https://doi.org/10.1007/s10518-014-9603-3.

[39] Sutton MA, Orteu JJ, Schreier H. Image Correlation for Shape, Motion and Deformation Measurements: Basic Concepts,Theory and Applications. Springer US;

2009.
[40] CEN. EN 1996-1-1 - Eurocode 6 - Design of masonry structures - Part 1-1: General rules for reinforced and unreinforced masonry structures. 2005.
[41] Tomaževič M. Earthquake-Resistant Design of Masonry Buildings. London: Imperial College Press; 2006.
[42] Rots JG, Messali F, Esposito R, Jafari S, Mariani V. Computational modelling of masonry with a view to Groningen induced seismicity. Struct Anal Hist Constr Anamn diagnosis, Ther Control - Proc 10th Int Conf Struct Anal Hist Constr. SAHC 2016, 2016, p. 227–38. https://doi.org/10.1201/9781315616995-29.
[43] TNO. DIANA Finite Element Analysis, User's Manual 2019.
[44] Federátion Internationale du Béton. The fib Model Code for Concrete Structures 2010. Wiley and Sons; 2013.
[45] Alger MSM. Polymer Science Dictionary. 3rd ed. Springer; 2017. https://doi.org/10.1007/978-94-024-0893-5.
[46] Drougkas A, Roca P, Molins C. Compressive strength and elasticity of pure lime mortar masonry. Mater Struct 2016;49. https://doi.org/10.1617/s11527-015-0553-2.